Polymer Melt Devolatilization Mechanisms

Scanning electron microscopy (SEM) was used to study the mechanism of falling-strand devolatilization of polymer melts. Polystyrene and low-density polyethylene were enriched with styrene and hexane, respectively, and were subsequently extruded as thin strands at various conditions. The polymer strands were exposed to superheat conditions for preset periods of time ranging from tenths to tens of seconds. The strands were then frozen, fractured, and studied by SEM. Devolatilization was found to proceed through a blistering mechanism, both on the surface of the strands and on the surfaces of volatile bubbles formed within the core of the melt. At all volatile concentrations surface blistering and foaming preceded bubble growth in the core, and occurred before the strands foamed. A mechanism for the observed polymer melt devolatilization is proposed.

Ramon J. Albalak
Zehev Tadmor
Yeshayahu Talmon
Department of Chemical Engineering
Technion, Israel Institute of Technology
Haifa 32000, Israel

Introduction

In the manufacturing process of most polymers there is a need to separate unreacted monomer, solvents, and other low molecular weight components from the polymer. Industrially this devolatilization step is carried out either in so-called falling-strand devolatilizers or in rotating devolatilizers (Biesenberger and Sebastian, 1983; Denson, 1985). The former are adaptations of ordinary flash tanks to high-viscosity molten polymers, and consist of vacuum tanks into which polymer melt is extruded in the form of thin strands. By the time the strands reach the bottom of the tank, their volatile content has been reduced. The principal types of rotating machine devolatilizers are vented single-screw extruders, intermeshing and nonintermeshing twin-screw extruders, the wiped-film evaporator, and the more recent corotating disk processors (Mehta et al., 1984).

At first, devolatilization in rotating equipment was considered to be a simple surface renewal and diffusion process, and was theoretically treated as such (Latinen, 1962; Roberts, 1970). However, diffusion coefficients calculated by Latinen from experimental data obtained from vented single-screw extruders were orders of magnitude larger than what could be expected for the styrene–polystyrene system examined, indicating that diffusion with surface renewal alone does not govern devolatilization. Further indication that devolatilization under vacuum in single-screw extruders is not a simple diffusive process was given by Biesenberger and Kessidis (1982). As suggested by them and others, it proved to be a more complex process involving boiling, foaming, and foam breaking. Direct visual observation in corotating disk processors also supports this notion (Mehta et al., 1984). The same holds in strand devolatilization. Indeed, Newman and Simon (1980) viewed the process of falling-strand devolatilization to be one of molecular diffusion into a swarm of bubbles, and expansion of those bubbles against surface tension and viscous forces. In their mathematical model they calculated the growth of a single bubble, and the corresponding volatile depletion in a unit volume of polymer melt. Their analysis was based on penetration theory, corrected for convective effects due to bubble expansion and the extended Rayleigh equation for bubble growth. Bubble nucleation was not considered, because they assumed that the devolatilizer is fed with a melt stream already swollen with vapor bubbles from the previous processing step. Bubble coalescence and rupture was assumed to occur suddenly and uniformly throughout the foamed-up solution. Their model compared favorably with experimental data from a polystyrene–styrene system in a temperature range of 200 to 250°C and with an initial concentration of styrene from 1,500 to 12,500 ppm. The growth of a diffusion-fed gas bubble in a viscous liquid medium had also been the subject of various earlier studies. Barlow and Langlois (1962), Szekely and Martins (1971), and Patel (1980) considered phase growth in viscous Newtonian liquids, while a non-Newtonian power-law fluid was the basis for a study by Street et al. (1971).

Our previous work (Albalak et al., 1987), however, indicates that strand devolatilization even transcends the complexity of a boiling mechanism involving nucleation, bubble growth, and rupture. Using scanning electron microscopy, several morphological structures were discovered which indicated that bubble

The current address of R. J. Albalak is Department of Materials Science and Engineering, Massachusetts Institute of Technology, Cambridge, MA 02139.

growth in polymer melts in general, and in particular foaming devolatilization do not progress through simple diffusion to small spherical bubbles, but rather through a complex series of steps. One of the features that appeared in samples extruded into high vacuum is swarms of randomly scattered, relatively large voids. These voids, termed macrobubbles, are of the order of 100 μm and above, and appear both in the core of the strand and on its lateral surface. It was found that the inner surface of a macrobubble is sometimes inhabited by blisters, which are thin, dome-shaped vapor-filled pockets. There are two distinctly different types of blisters:

microblisters, 1 to 3 μm dia.

miniblisters, 10 to 15 μm dia.

Microblisters and miniblisters frequently appear side by side, and our previous work presented a detailed account of how they evolve from each other. It was suggested that a first generation of microblisters emerges through the soft molten surface of a macrobubble after having been formed as tiny microbubbles under the surface. These vapor-filled microblisters grow to a maximum diameter of about 3 μm, at which stage the skin containing the vapor is too thin and therefore too weak to withstand the pressure difference; it bursts, releasing the contained vapor to the macrobubble. If microblisters emerge close enough to each other they may merge to form a larger structure, a miniblister. At some stage the miniblister also bursts and the nearly empty skin collapses, entrapping small vapor-filled pockets which become the nucleation sites for a second generation of microblisters growing on the remains of the previous-generation miniblister.

Experimental work has continued, concentrating on the initial stages of devolatilization. In this paper we suggest a model to explain the formation of satellite microbubbles that blister into the surface of a growing macrobubble. Heterogeneous nucleation of bubbles in polymer melts is examined, and the effect of superheat and tensile stress on its rate is analyzed.

Experimental Method

The experimental system used is a modified version of that used in our previous work. The system consists of a melt flow indexer (MFI) that produces the polymer melt, and a heated brass devolatilization chamber into which a thin strand of melt is extruded through a die. Figure 1 is a drawing of the experimental system. The devolatilization chamber includes connections to vacuum and cooling-water systems, and two viewing ports through which strand extrusion is viewed and videotaped. The chamber is connected to the vacuum and cooling systems through timer-controlled solenoid valves, which enable the chamber to be evacuated for a preset period of time before being flooded with water. The vacuum system includes a 30 L evacuated tank for fast evacuation of the 0.2 L devolatilization chamber.

Polymer pellets are fed into the MFI through its funnel-shaped top and are compressed by a plunger loaded with weights. The molten polymer is extruded into the devolatilization chamber, initially at 235°C and atmospheric pressure. At these conditions, the volatiles in the polymer are not superheated. The extrusion process is observed through the viewing port. After a strand of some 10 cm is formed, the control system is activated.

As the control system is operated, the solenoid valve connecting the chamber and the vacuum system is opened for a preset

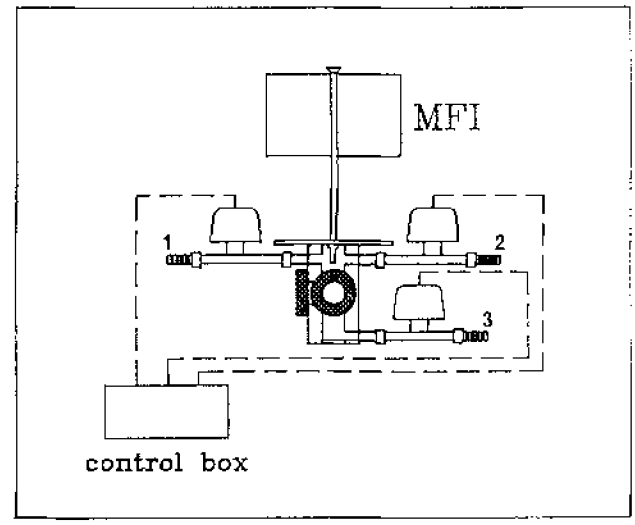

Figure 1. Experimental system.

(1) Connection to vacuum system; (2) connection to incoming cooling water; (3) cooling water drainage

time. The periods of time set ranged from 0.6 to 28.0 s. While the valve is open the polymer strand within the chamber is subjected to pressure in the range of 130–400 Pa (1–3 mm Hg), and the polymer–volatile solution is immediately superheated, as indicated in Figure 2, which shows the equilibrium partial pressure of the volatiles in the polymeric systems used. As the vacuum valve is shut, the valve connecting the chamber to the incoming cooling water is opened, and a split second later the drain valve is opened, allowing circulation of cooling water through the chamber. The flow of water freezes the polymer strand, preserving the microstructure formed during devolatilization.

After freezing, scanning electron microscope samples were prepared. The frozen strands were detached from the die and fractured in liquid nitrogen to reveal their cross-sections. The segments of the strands were cemented to cylindrical specimen holders, and sputter-coated with a 25 nm gold layer. The specimens were examined in a JEOL T-300 scanning electron

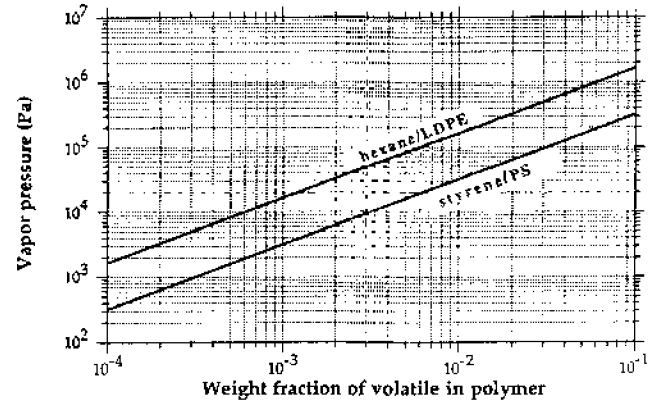

Figure 2. Equilibrium vapor pressure of styrene in a styrene–polystyrene solution and hexane in a hexane–LDPE solution at 235°C.

According to Flory-Huggins theory with an interaction parameter $\chi = 0.42$, chosen according to Werner (1980)

microscope in the secondary electron imaging (SEI) mode, using an electron acceleration voltage of 25 kV. The cross sections and lateral surfaces of the specimens were examined at magnifications of up to 35,000× .

The materials used in this study were a general-purpose polystyrene (PS 5E242, British Petroleum) and low-density polyethylene (LDPE 111, Israeli Petrochemical Enterprises) that were enriched with styrene and hexane, respectively, by vapor adsorbtion. A single layer of weighed pellets was placed in a Petri dish which was placed in a vacuum oven at 70°C for 24 h to ensure a volatile-free starting point. The Petri dish was then transfered to a dessicator, the bottom of which contained the liquid volatile. The dessicator was placed in an oven at 50°C for 30 min, and was then left closed overnight at room temperature. The volatile concentrations reached at this stage were higher than required, and superflous volatiles were removed in a vacuum oven to obtain the desired final concentration. Polystyrene with an initial concentration of 300 ppm styrene was enriched to 10,000 ppm styrene, and low-density polyethylene was enriched with hexane to various concentrations up to 30,000 ppm.

Results

The first series of experiments was conducted using polystyrene with an initial concentration of 300 ppm styrene. Figure 3a shows a scanning electron micrograph of a sample exposed to a pressure of 270 Pa (~2 mm Hg) for 0.6 s. The lateral surface of the strand and its cross section show no evidence of foaming or blistering, and appear to be featureless on both macroscopic and microscopic scales. Microblistering of the lateral surface was the first evidence of devolatilization, and was encountered on specimens exposed to vacuum for 0.8 s. Similar morphological structures were found on strands exposed to vacuum for up to 6.0 s. Figure 3b shows blister remains on the lateral surface of a strand superheated for 1.4 s. The different size indentations in the strand surface correspond to microblisters (~1 μm) and miniblisters (~5–15 μm). Figure 3c shows the lateral surface of a strand exposed to vacuum for 2.2 s. Overlapping tracks indicate that several generations of blisters have evolved by this time. At the bottom right of the micrograph the remains of a large blister can be seen to overlap four smaller tracks of some 10 μm dia. each. The area enclosed by this feature seems to be smooth in comparison to the surroundings, indicating volatile depletion due to the formation of the large blister (~20 μm dia.). The surrounding surface, apparently still rich with volatiles, continues to form additional generations of microblisters. After 6.0 s of superheat, the strand is still macroscopically smooth, Figure 3d, although microblistering on the lateral surface is intense, as seen in Figure 3e. Although single macrobubbles were encountered on the lateral surface of strands as early as 1.4 s of superheat, only after 7.3 s of vacuum exposure is macroscopic foaming of the extruded strands detected. Foaming appears on the blistered lateral surface of the strand, Figure 3f, while the cross section at this stage exhibits only single macrobubbles, Figure 3g. Figure 3h shows that these bubbles are covered with blister remains. Samples examined after 8.5 s of superheat look the same. Complete foaming of the core of the polymer strands occurs only after being exposed to superheat for at least 9.6 s, Figure 3i.

A second series of experiments was conducted using polystyrene containing an initial concentration of 10,000 ppm styrene.

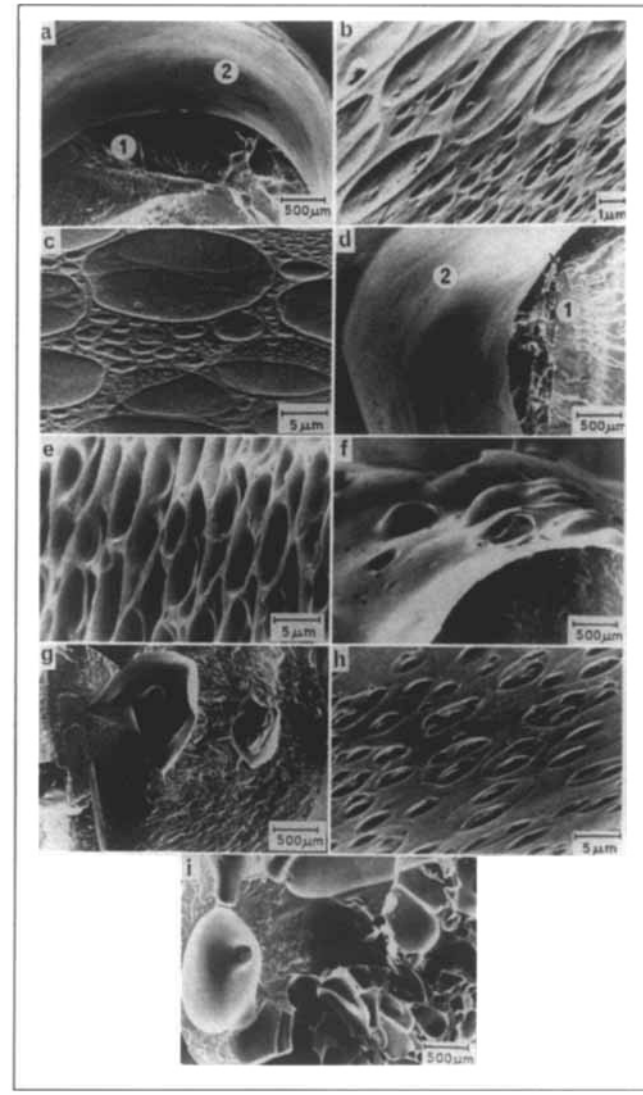

Figure 3. Scanning electron micrographs of polystyrene strands with an initial concentration of 300 ppm styrene superheated for different periods of time.

(a) 0.6 s: 1. cross-section; 2. lateral surface
(b) Blister remains on lateral surface after 1.4 s
(c) Blister remains on lateral surface after 2.2 s
(d) After 6.0 s: 1. cross section; 2. lateral surface
(e) Blister indentations on lateral surface after 6.0 s
(f) Foamed lateral surface after 7.3 s
(g) Single bubbles on cross section after 7.3 s
(h) Blister tracks on a macrobubble surface on cross section after 7.3 s
(i) Foamed cross section after 9.6 s

Figure 4a shows that after only 0.8 s of superheating, the lateral surface of the strand is swollen with macrobubbles. Figure 4b shows blistering on the lateral surface of the same strand at a higher magnification. Bubble growth in the core is also found to occur after shorter vacuum exposure than with 300 ppm styrene. Figure 4c shows blistering on the surface of a macrobubble formed on the cross section of a strand exposed to vacuum for 0.8 s. Similar features were found on samples with an initial 300 ppm styrene concentration only after 7.3 s of superheating. After being exposed to vacuum for 2.2 s, the strands are

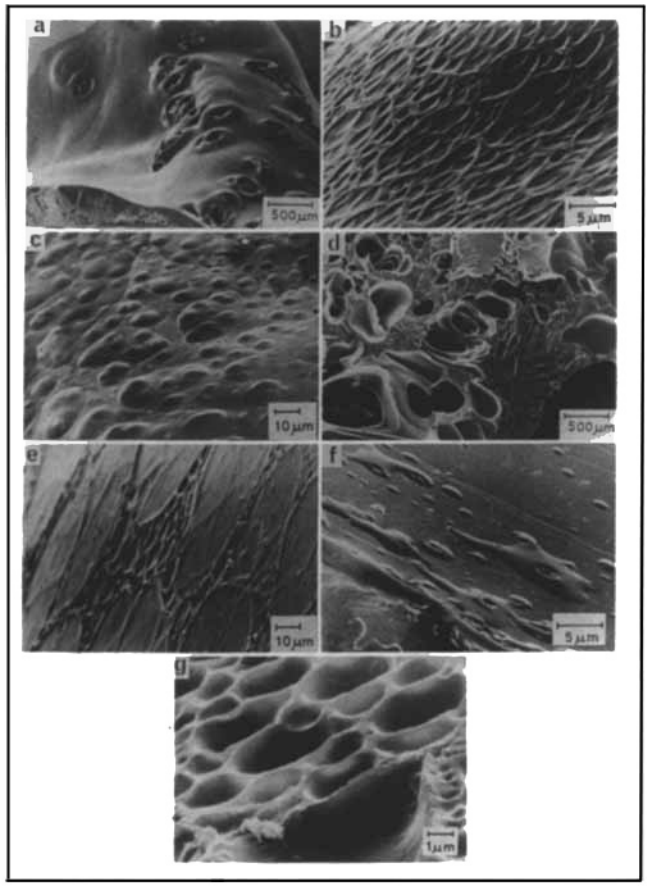

Figure 4. Scanning electron micrographs of polystyrene strands with an initial concentration of 10,000 ppm styrene superheated for different periods of time.

(a) Foamed lateral surface after 0.8 s
(b) Blistering on lateral surface after 0.8 s
(c) Blister tracks on a macrobubble surface on cross section after 0.8 s
(d) Foamed cross section after 2.2 s
(e) Blister remains on lateral surface after 2.2 s
(f) Blisters on macrobubble surface on cross section after 2.2 s
(g) Blister indentations on lateral surface after 4.7 s

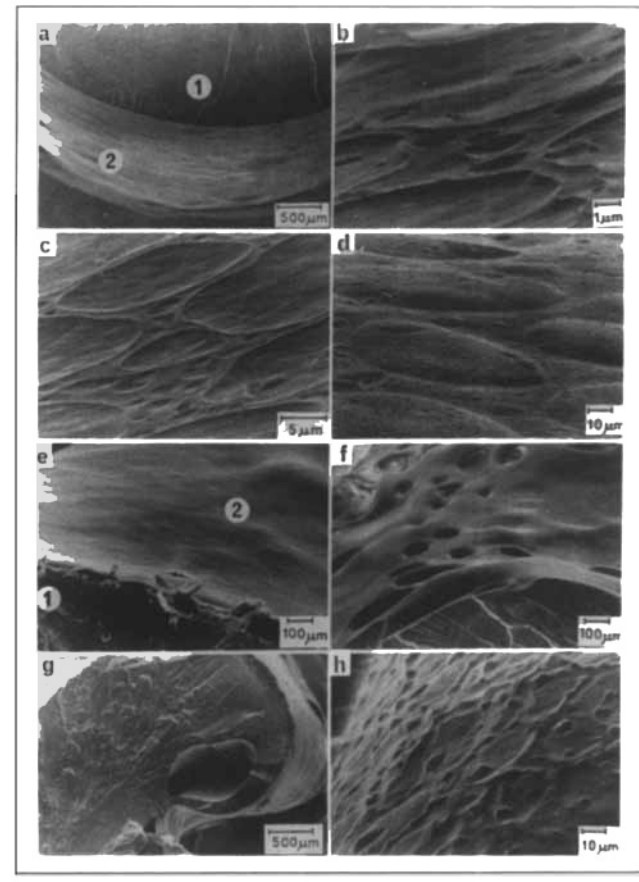

Figure 5. Scanning electron micrographs of polyethylene strands with an initial concentration of 4,000 ppm hexane superheated for different periods of time.

(a) After 0.6 s: 1. cross section; 2. lateral surface
(b) Blister remains on lateral surface after 0.6 s
(c) Blister remains on lateral surface after 0.8 s
(d) Blister remains on lateral surface after 2.2 s
(e) After 6.0 s: 1. cross section; 2. lateral surface
(f) Foamed lateral surface after 9.6 s
(g) A single macrobubble on cross section after 9.6 s
(h) Blistering on a macrobubble surface on cross section after 9.6 s

completely foamed, Figure 4d; the lateral surface displays the remains of several blister generations, Figure 4e. Evidence of blistering is also found on bubble surfaces in the cross section, as shown in Figure 4f. By the time 4.7 s of superheat have elapsed, surface blistering has become more intense, leaving the deeper indentations shown in Figure 4g.

Similar experiments were conducted with low-density polyethylene enriched to various concentrations of hexane. Figures 5 and 6 consist of micrographs of low-density polyethylene strands with an initial concentration of 4,000 ppm hexane, that were exposed to vacuum for various times up to 28.0 s. Figure 5a shows the cross section and lateral surface of such a strand after being superheated for 0.6 s. The macroscopic appearance of the strand is similar to that of the polystyrene strand of Figure 3a, and exhibits no evidence of foaming. However, taking a closer look at the lateral surface of the strand, Figure 5b, shows that on the microscopic scale blistering has already begun. Microblistering of the lateral surface becomes more intense with longer exposure to superheated conditions, as is evident from Figures 5c and 5d which respectively show strands after 0.8 and 2.2 s of superheat. It can be seen from Figure 5d that a later generation of microblisters has sprouted, and seems to cover the previous generations of microblisters and miniblisters. Figure 5e shows a strand after 6.0 s exposure to vacuum, and both the cross section and lateral surface are still featureless on the macroscopic scale. Only after being exposed to superheat conditions for 9.6 s does there appear to be any foaming of the strand's lateral surface, Figure 5f. After this period of time some of the strands extruded begin to exhibit single macrobubbles in the core, Figure 5g. On closer inspection these bubbles show evidence of blistering, Figure 5h. The intensity of lateral surface microblistering continues to grow, as does the size of the blisters found after 12.6 s exposure to vacuum, Figure 6a. After 16.9 s of superheat, all the strands examined exhibited macrobubbles on their cross sections, Figure 6b, and, as expected, the bubble surfaces showed evidence of blistering, Figure 6c. By this time, the lateral surfaces of the strands had completely foamed, Figure 6d. After 28.0 s exposure to vacuum the entire cross section of

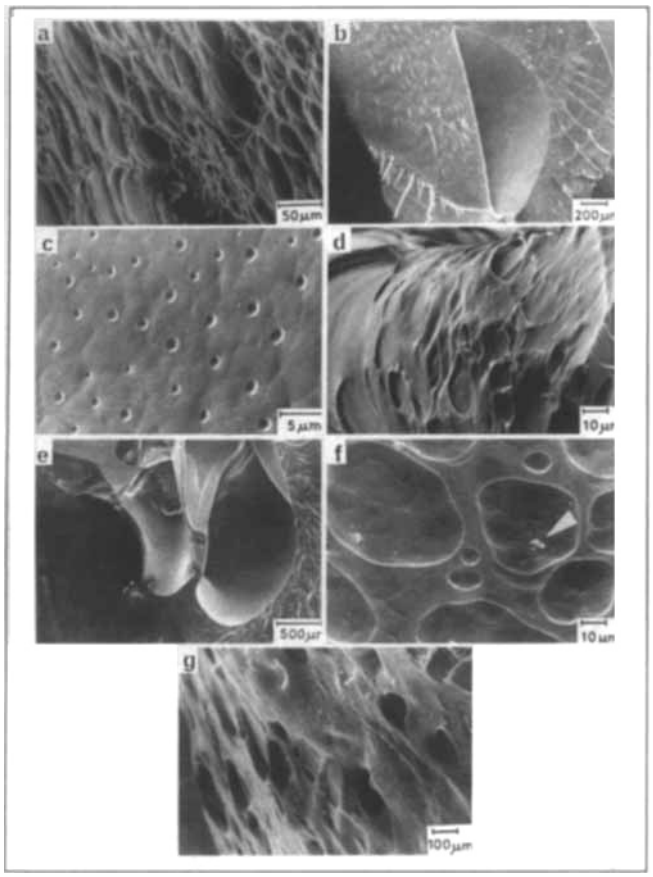

Figure 6. Scanning electron micrographs of polyethylene strands with an initial concentration of 4,000 ppm hexane superheated for different periods of time.

(a) Blister remains on lateral surface after 12.6 s
(b) A macrobubble on cross section after 16.9 s
(c) Blistering on a macrobubble surface on cross section after 16.9 s
(d) Foamed lateral surface after 16.9 s
(e) Foamed cross section after 28.0 s
(f) Blistering on a macrobubble surface on cross section after 28.0 s; arrow indicates a dust particle
(g) Foamed lateral surface after 28.0 s

the strand is foamed, as shown in Figure 6e. On the microscopic scale the remains of various sized blisters can be seen, Figure 6f. Figure 6g shows the extent of lateral surface foaming after 28.0 s.

Proposed Mechanism and Discussion

It is suggested that initial blistering and foaming occur on the lateral surface for a number of reasons. The first is the immediate contact the surface has with the surrounding vacuum, as opposed to an undetermined pressure within the core of the strand. Any bubble growth within the strand must overcome the energy required to displace viscous material to form a void, whereas blistering on the surface does not encounter such resistance. Moreover, blister growth, which is observed to be a rapid process, may occur within the strand only after a microbubble has nucleated and initially grown by diffusion. A possible additional reason for intensive activity on the lateral surface of the strands is the continuous bombardment of the surface by minute dust particles found in the atmosphere. These particles are present even at the moderate vacuum at which industrial devolatilization is performed, and are certainly present in our experiments in which strands are extruded into the vacuum chamber initially at atmospheric pressure. On impact with the melt these particles may form heterogeneous nucleation sites for bubble–blister growth. Indeed, impurities such as dust particles were found on the strands, and are indicated by the arrow in Figure 6f.

Turning to the core of the strand, it is evident that the overall mechanisms for blistering and bubble growth on the lateral surface and in the core are not identical, although certain basic stages are shared by both. As soon as the polymer strand is superheated, microbubbles should begin to nucleate in the core of the melt.

The generally accepted model for heterogeneous nucleation in the core of the liquid is that of Harvey et al. (1944a, b), who studied bubble formation in superheated biological systems and who postulated the existence of entrained microparticles (e.g., dust particles) themselves containing acute-angle microcrevices. According to the Laplace equation:

$$P_v - P_l = \frac{-2\sigma}{R} \tag{1}$$

the pressure in a gas pocket in such a microcrevice, Figure 7, is less than that of the liquid. The deeper the liquid penetrates into the cavity, the smaller the gas pressure becomes, until a value must be reached at which the gas pressure in the crevice is at equilibrium with the dissolved gas. Hence conditions for stable nuclei exist.

The rate of heterogeneous bubble nucleation in superheated systems was presented by Blander and Katz (1975), based on the work of Fisher (1948):

$$J = N^{2/3} S \left[\frac{2\sigma}{\pi MBF}\right]^{1/2} \exp\left[\frac{-16\pi\sigma^3 F}{3kT(P_v - P_l)^2}\right] \tag{2}$$

They have shown that the difference between the pressure in the bubble, P_v, and the pressure in the surrounding melt, P_l, can be expressed in terms of the superheat $P_s - P_l$ by the following

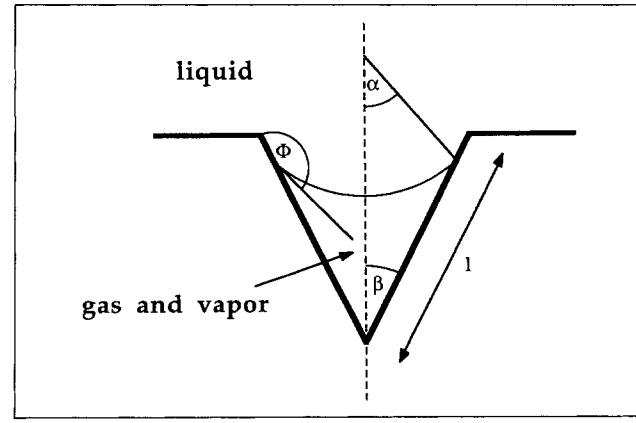

Figure 7. A stable Harvey-type nucleus in a conical cavity.

expression:

$$P_v - P_l \approx (P_s - P_l)\delta \tag{3}$$

where the Poynting correction factor, δ, is very close to 1.

By substituting Eq. 3 into the exponential term of Eq. 2, it can be seen how an increase in the superheat of the polymer–volatile system (e.g., by raising the volatile content) increases the rate of nucleation.

For conical cavities, such as those discussed by Harvey et al., Cole (1974) has developed the following expression for the geometric parameter F that appears in Eq. 2.

$$F = \frac{3}{2}\left[(1 - \cos\alpha) + \frac{1}{2}\left(\frac{l}{R_c}\right)^2 \sin\beta \cdot \cos\Phi\right] - \frac{1}{2}\left[(1 - \cos\alpha)^2 \cdot (2 + \cos\alpha) + \left(\frac{l}{R_c}\right)^3 \sin\beta \cdot \cos\beta\right] \tag{4}$$

The cavity depth, l, and the angles α, β, and Φ are defined in Figure 7; R_c is the critical radius of a vapor bubble at the melt temperature. The values of F vary in this case from 0.0 to 0.5, and are highly sensitive to the geometry of the cavity and the wetting angle Φ. Since the geometry of any dust particles present in the system is unknown, the true value of F is uncertain, and reliable calculations of the nucleation rate using Eq. 2 are not possible. However, the equations are useful in pointing toward the possible effect of various parameters.

An attempt was made to experimentally calculate macrobubble nucleation rates from low-magnification micrographs showing large portions of the cross section, assuming that each macrobubble represents the activation of a single nucleation site. The calculation also assumes that the bubble density in a plane perpendicular to the cross section, the rz plane, is similar to that of the $r\theta$ cross sectional plane shown in the micrograph. This asumption makes it possible to calculate the number of macrobubbles in a given volume of melt. Thus, for a polystyrene strand with an initial concentration of 300 ppm styrene, the density of bubbles found, using Figure 3i, was on the order of 20,000 bubbles $\cdot$ cm^{-3}. Calculating the rate of nucleation presents a more difficult problem, since we cannot be sure of the length of time in which these bubbles nucleated. Although the exposure time of the strand was known to be 9.6 s, it is not clear if nucleation starts as soon as the strand is superheated. Nucleation may possibly begin much later, since the earliest bubbles were found only after 7.3 s, Figure 3g. Assuming that bubbles nucleate as soon as the strand is superheated results in a calculated nucleation rate of 2,000 nuclei $\cdot$ cm^{-3} $\cdot$ s^{-1}. Taking the nucleation period to be as short as 0.1 s results in a much higher rate of 200,000 nuclei $\cdot$ cm^{-3} $\cdot$ s^{-1}. Based on similar assumptions, the experimental nucleation rates calculated from Figure 4d for polystyrene with an initial concentration of 10,000 ppm styrene range from 10,000 to 200,0000 nuclei $\cdot$ cm^{-3} $\cdot$ s^{-1}, and the rates calculated from Figure 6c for polyethylene with an initial concentration of 4,000 ppm hexane range from 100 to 40,000 nuclei $\cdot$ cm^{-3} $\cdot$ s^{-1}.

Equation 2 expresses the rate at which *primary* microbubbles nucleate in the melt. Primary microbubbles are those that are formed in the polymer melt before any blistering occurs, and which finally grow to form the macrobubbles found in the core of the strands. Microbubbles grow by two mechanisms:

1. Diffusion of volatiles from the surrounding melt
2. Formation of blisters on the bubble surface, subsequent blister rupture, and release of volatiles to the interior of the bubble.

The blistering process is, in essence, the coalescence of a primary bubble with the many *secondary* microbubbles formed around it. These secondary microbubbles nucleate at a much higher rate than the primary microbubbles. The actual rate at which secondary microbubbles nucleate and form blisters on the surface of a growing macrobubble has also been estimated from micrographs, and found to be much higher than the nucleation rate of the macrobubbles themselves, reaching values on the order of 10^{11} $\cdot$ cm^{-3} $\cdot$ s^{-1}. The increase in the nucleation rate is hypothesized to be due to the additional superheat caused by the build-up of negative pressure during bubble growth.

Raising the volatile content has the effect of increasing the equilibrium vapor pressure, P_s, causing an increase in the degree of superheat expressed as $P_s - P_l$. Alternatively, the degree of superheat may be raised by lowering the value of P_l. Subjecting the system to external vacuum may reduce P_l to a minimum value close to zero. Further decrease in the local value of P_l may occur by a cavitation process due to tensile stress generated by the moving boundary of an existing growing gas macrobubble in the liquid medium.

Street (1968) showed that the angular stresses at the bubble surface in a viscoelastic liquid are given by

$$\tau_{\theta\theta} = \tau_{\phi\phi} = -\left\{\frac{2\mu_0\dot{R}}{R} + \left(\frac{4\mu_0\alpha^2\lambda_1}{1 - 2\alpha\lambda_1}\right)\left[1 - e^{-(1-2\alpha\lambda_1)(t/\lambda_1)}\right]\right\} \tag{5}$$

in which μo is the zero-shear viscosity, λ_1 is the first relaxation time, which vanishes for Newtonian fluids, and $\alpha = \dot{R}/R$. Equation 5 shows that at the bubble surface there are tensile stresses in the θ and ϕ directions.

Adding the tensile stress contribution to the superheat term $(P_s - P_l)$ in the expression for primary bubble nucleation gives an expression for the rate at which secondary bubbles nucleate. The significance of this contribution has been estimated from Eq. 5 for a macrobubble of 200 μm dia. growing in a Newtonian liquid. The melt viscosity was taken as 5,000 Pa $\cdot$ s, and $\dot{R}$ was assumed to be 100 μm/s. The angular stresses resulting in such a case are on the order of 10,000 Pa, which is in agreement with the results of Han and Yoo (1981) who calculated stress build-up in a similar system. Comparing this figure to the superheat of a 300 ppm styrene–polystyrene solution at 235°C at a surrounding pressure of 130 Pa (1 mm Hg), which is about 900 Pa, demonstrates the important role tensile stresses may have in determining the secondary microbubble nucleation rate. However, as the superheat of the polymer–volatile system increases (e.g., 32,000 Pa for polystyrene containing 10,000 ppm styrene) the relative importance of the additional superheat due to tensile stresses may decrease.

The build-up of tensile stresses in the liquid adjacent to a growing bubble may activate preferentially oriented nuclei that would remain inactive at the surrounding pressure, thus forming a large number of satellite microbubbles. Because the original bubble continues to grow toward these microbubbles, they eventually coalesce with it in the form of a first generation of

microblisters on the inner surface of the larger bubble. This process is presented in Figure 8. The next state is the cyclic repetition of the previously discussed blistering mechanism, forming several generations of microblisters and miniblisters. Another reason for the high rate of secondary microbubble nucleation is the possible accumulation of solid particles by the surface of the growing macrobubble; impurities that are initially randomly distributed in the polymer melt tend to be picked up by the advancing bubble front, resulting in more potential nucleation sites at the bubble surface. This way volatile bubble growth in a viscoelastic medium can easily become an autocatalytic process. Once primary bubbles begin to grow via blistering in addition to diffusion, bubble growth is accelerated, and adjacent macrobubbles will start to coalesce, thus rapidly foaming the entire cross section.

The sequence of events on the lateral surface differs in some respect from the above mechanism proposed for the core of the strands. Since blisters can form only on a free surface, blistering in the core is inhibited until bubble surfaces are formed. The lateral surface, however, may blister as soon as a first generation of microbubbles nucleates on the surface. As we have already stated, there are several reasons for a high nucleation rate on the lateral surface, and earlier microbubble formation. Since the microbubbles nucleate on the surface (or very close under it) they are actually the first generation of microblisters, after which additional generations of microblisters and miniblisters may form, as they do in the core of the strands. Cyclic repetition of blister formation and merging causes depletion of the volatiles from the surface crust, usually leaving a foamed surface.

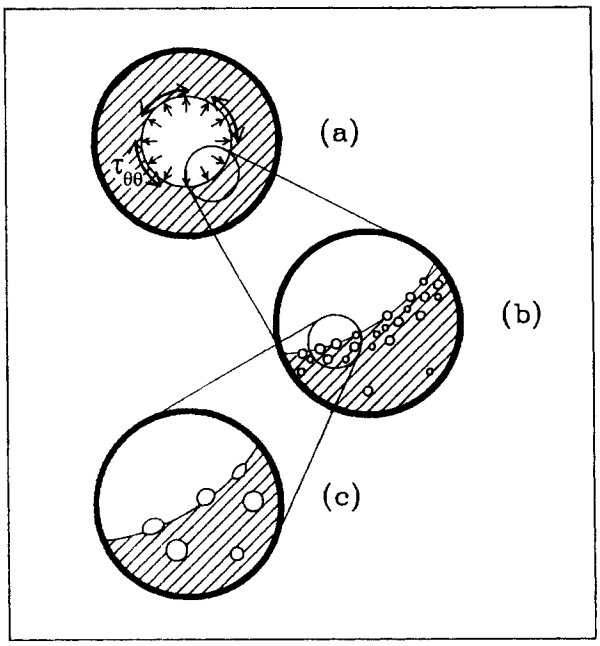

Figure 8. Mechanism in the core.

(a) A growing macrobubble generates angular stresses in surrounding melt
(b) Secondary microbubbles nucleate around macrobubble due to local reduction in pressure and coalesce with it, forming blisters on inner surface of macrobubble
(c) Detail of (b)

Conclusions

A general mechanism for falling-strand devolatilization has been presented in which we have shown that heterogeneous bubble nucleation in the core plays a major role in determining the overall rate of devolatilization. The degree of superheat of the polymer solution and the geometry of available nucleation sites were shown to govern the heterogeneous nucleation rate. Additionally, tensile stresses accompanying bubble growth may result in a local increase of superheat. This additional superheat, combined with the possible accumulation of impurities on the macrobubble surface, may be sufficient to increase the nucleation rate of microbubbles in the melt adjacent to the growing bubble, resulting in the large number of blisters formed on the bubble surface.

Although the mechanism proposed is based on microstructures formed during falling-strand devolatilization, there is reasonable basis to assume that some or all of the features observed in this study also play a role in rotating devolatilizers. There is also some basis to believe that similar phenomena may occur during other operations involving the vaporization of liquids, such as the spray-drying of foods. We hope that our present study may serve food scientists in achieving a better understanding of spray-drying processes and encourage them to conduct microscopic studies that are more detailed than those currently appearing in the literature.

Because rotary devolatilization equipment is characterized by high shear fields, bubble nucleation, coalescence, and rupture are expected to occur at higher rates than in the falling-strand process. Work along these lines is being carried out in our laboratories.

Acknowledgment

The authors gratefully acknowledge support for this research by a grant from the German-Israeli Foundation for Scientific Research and Development (GIF). They also thank Judith Schmidt and Bertha Shdemati for their contribution to this research.

Notation

B = coefficient, Eq. 2
F = geometrical factor of nucleation site, $0 < F < 1$
J = heterogeneous nucleation rate
k = Boltzman's constant
l = cavity depth, Figure 7
M = molecular weight
N = number density of liquid
P_l = pressure in the liquid medium
P_s = equilibrium vapor pressure of volatile in polymeric solution
P_v = pressure of vapor in a bubble
r = radial coordinate
R = bubble radius
R_c = critical bubble radius
S = geometric factor of nucleation site
t = time
T = temperature

Greek letters

α = angle, Figure 7
$\alpha = \dot{R}/R$
β = angle, Figure 7
δ = Poynting correction factor
θ = angular coordinate
λ_1 = first relaxation time
μ = melt viscosity
μ_0 = zero shear viscosity

ρ_g = density of gaseous phase
ρ_l = density of liquid phase
σ = surface tension
τ_{rr} = radial normal stress
$\tau_{\theta\theta}$ = angular normal stress
$\tau_{\phi\phi}$ = angular normal stress
ϕ = angular coordinate
Φ = wetting angle
χ = Flory–Huggins interaction parameter

Literature Cited

Albalak, R. J., Z. Tadmor, and Y. Talmon, "Scanning Electron Microscopy Studies of Polymer Melt Devolatilization," *AIChE J.*, **33,** 808 (1987).

Barlow, E. J., and W. E. Langlois, "Diffusion of Gas from a Liquid into an Expanding Bubble," *IBM J. Res. Dev.*, **24,** 329 (1962).

Biesenberger, J. A., and G. Kessidis, "Devolatilization of Polymer Melts in Single-Screw Extruders," *Polym. Eng. Sci.*, **22,** 832 (1982).

Biesenberger, J. A., and D. H. Sebastian, *Principles of Polymerization Engineering,* Wiley, New York (1983).

Blander, M., and J. L. Katz, "Bubble Nucleation in Liquids," *AIChE J.*, **21,** 833 (1975).

Cole, R., "Boiling Nucleation," *Adv. Heat Transfer,* **10,** 85 (1974).

Denson, C. D., "Stripping Operations in Polymer Processing," *Advances in Chemical Engineering,* **12,** J. Wei, ed., Academic Press, New York, 61 (1985).

Fisher, J. C., "The Fracture of Liquids," *J. Appl. Phys.*, **19,** 1062 (1948).

Han, C. D., and H. J. Yoo, "Studies on Structural Foam Processing. IV: Bubble Growth During Mold Filling," *Polym. Eng. Sci.*, **21,** 518 (1981).

Harvey, E. N., D. K. Barnes, W. D. McElroy, A. H. Whiteley, D. C. Pease, and K. W. Cooper, "Bubble Formation in Animals. 1: Physical Factors," *J. Cellular Comp. Physiol.*, **24,** 1 (1944a).

Harvey, E. N., A. H. Whiteley, W. D. McElroy, D. C. Pease, and D. K. Barnes, "Bubble Formation in Animals. 2: Gas Nuclei and Their Distribution in Blood and Tissues," *J. Cellular Comp. Physiol.*, **24,** 23 (1944b).

Latinen, G. A., "Devolatilization of Viscous Polymer Systems," *Adv. Chem. Ser.*, **34,** 235 (1962).

Mehta, P. S., L. N. Valsamis, and Z. Tadmor, "Foam Devolatilization in Multichannel Corotating Disk Processors," *Polym. Process Eng.*, **2,** 103 (1984).

Newman, R. E., and R. H. S. Simon, "A Mathematical Model of Devolatilization Promoted by Bubble Formation," *AIChE Meet.*, Chicago (1980).

Patel, R. D., "Bubble Growth in a Viscous Newtonian Liquid," *Chem. Eng. Sci.*, **35,** 2352 (1980).

Roberts, G. W., "A Surface Renewal Model for the Drying of Polymers During Screw Extrusion," *AIChE J.*, **16,** 878 (1970).

Street, J. R., "The Rheology of Phase Growth in Elastic Liquids," *Trans. Soc. Rheol.*, **12,** 103 (1968).

Street, J. R., A. L. Fricke, and L. P. Reiss, "Dynamics of Phase Growth in Viscous, Non-Newtonian Liquids," *Ind. Eng. Chem. Fundam.*, **10,** 54 (1971).

Szekely, J., and G. P. Martins, "Non-Equilibrium Effects in the Growth of Spherical Gas Bubbles," *Chem. Eng. Sci.*, **26,** 147 (1971).

Werner, H., "Devolatilization of Polymers in Multiscrew Devolatilizers," *Devolatilization of Plastics,* (trans. from German), VDI-Verlag, Düsseldorf, FRG, 99 (1980).

Manuscript received Jan. 3, 1990, and revision received June 12, 1990.